

MoniRefer: A Real-world Large-scale Multi-modal Dataset based on Roadside Infrastructure for 3D Visual Grounding

Panquan Yang¹ Junfei Huang¹ Zongzhangbao Yin¹ Yingsong Hu¹
 Anni Xu¹ Xinyi Luo¹ Xueqi Sun¹ Hai Wu² Sheng Ao^{1†}
 Zhaoxing Zhu¹ Chenglu Wen¹ Cheng Wang^{1†}
¹Xiamen University ²Pengcheng Laboratory

Abstract

*3D visual grounding aims to localize the object in 3D point cloud scenes that semantically corresponds to given natural language sentences. It is very critical for roadside infrastructure system to interpret natural languages and localize relevant target objects in complex traffic environments. However, most existing datasets and approaches for 3D visual grounding focus on the indoor and outdoor driving scenes, outdoor monitoring scenarios remain unexplored due to scarcity of paired point cloud-text data captured by roadside infrastructure sensors. In this paper, we introduce a novel task of **3D Visual Grounding for Outdoor Monitoring Scenarios**, which enables infrastructure-level understanding of traffic scenes beyond the ego-vehicle perspective. To support this task, we construct **MoniRefer**, the first real-world large-scale multi-modal dataset for roadside-level 3D visual grounding. The dataset consists of about 136,018 objects with 411,128 natural language expressions collected from multiple complex traffic intersections in the real-world environments. To ensure the quality and accuracy of the dataset, we manually verified all linguistic descriptions and 3D labels for objects. Additionally, we also propose a new end-to-end method, named **Moni3DVG**, which utilizes the rich appearance information provided by images and geometry and optical information from point cloud for multi-modal feature learning and 3D object localization. Extensive experiments and ablation studies on the proposed benchmarks demonstrate the superiority and effectiveness of our method. Our dataset and code will be released.*

1. Introduction

3D visual grounding(3DVG) aims at localizing a referred target object in 3D scenes based on a given referring expressions. By establishing an intrinsic connection between

linguistic expressions and corresponding visual elements, it enables intelligent systems and embodied agents to possess human-like comprehensive understanding and reasoning ability. 3DVG is emerging as a frontier research direction across various domains, including autonomous driving [8, 31, 53, 60], embodied intelligence [56, 58, 61], vision-language-action [20, 30, 63], vision-and-language navigation [2, 7, 37], and surveillance [21, 71, 72, 81].

In recent years, visual grounding in 2D scenes [14, 28, 38, 52, 66, 67, 74] has made significant progress, due to the availability of a large amount of datasets [46, 47, 73]. However, these methods and datasets are constrained to the 2D domain and cannot capture the true 3D content of objects, making it difficult to directly extend these 2D approaches to the 3D setting. Recent many efforts [19, 27, 42, 62, 75, 78] have primarily focused on indoor benchmarks [1, 6], where sensing range of RGB-D camera is up to 5 meters and the pre-scanned indoor scenarios is static. It has certain limitations in handling dynamic, complex, large-scale and ever-changing outdoor scenarios.

Therefore, several works [10, 15, 32, 76] have investigated 3DVG for autonomous driving by leveraging paired linguistic descriptions and visual data, enabling automated vehicles to identify referred targets in driving scenes. Other efforts [34] have explored human-centric environments, revealing significant potential for the advancement of human–robot interaction. However, distinct from these settings, 3D visual grounding from roadside surveillance perspectives remains unexplored and faces several key challenges: (1) Data scarcity. LiDAR–text paired data is extremely limited in roadside monitoring scenarios. Most outdoor 3DVG datasets are derived from autonomous driving benchmarks [4, 18], which contain relatively few objects and focus primarily on vehicles, while underrepresenting vulnerable road users (VRUs) such as pedestrians and cyclists that are critical for situational awareness. (2) Limited linguistic diversity and richness: Existing descriptions are typically brief and coarse, lacking detailed references to object attributes and contextual relationships. Richer and

[†]Corresponding author.

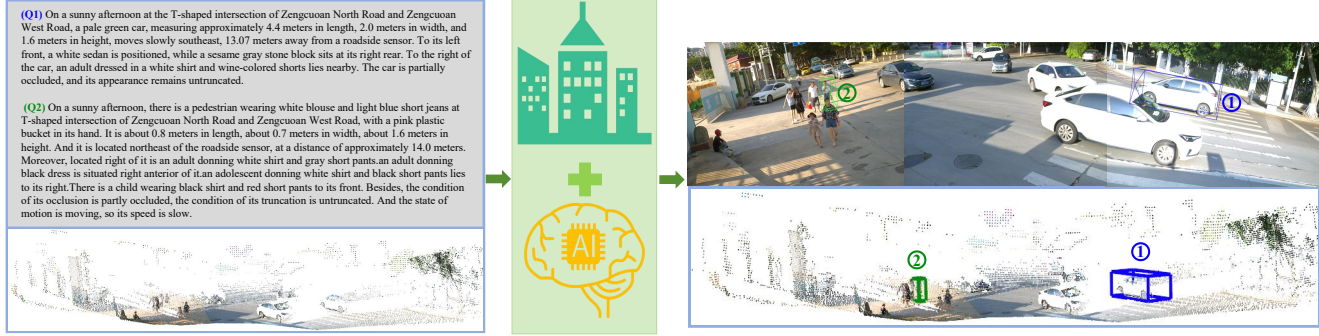


Figure 1. **Introduction to 3D Visual Grounding for Outdoor Monitoring Scenarios.** Moni3DVG integrates multi-modal visual data collected from roadside infrastructure sensors with natural language descriptions to localize the referred object in highly dynamic and complex traffic environments. For clearer visualization, the localization results are also presented in the corresponding images.

more discriminative language is crucial for resolving object ambiguities in crowded or complex scenes. (3) Perspective inconsistency: the roadside sensors are usually higher and perspectives are typically downward-looking, leading to inconsistent data distribution. In vehicle-mounted systems, limited receptive fields and blind spots caused by occlusion degrade localization accuracy, e.g., ghost probes at busy traffic intersections. In contrast, roadside sensors provide a broader and more stable field of view that enhances perception reliability and safety in intelligent transportation systems. Consequently, existing 3DVG datasets and methods often struggle to generalize effectively to outdoor monitoring environments.

To tackle these challenges, we introduce a novel task of **3D Visual Grounding for Outdoor Monitoring Scenarios**, which utilize linguistic descriptions and visual data collected from roadside infrastructure sensors to localize target objects in 3D space, as depicted in Fig.1. To support this task, We build the first real-world large-scale multi-modal dataset for roadside-level 3D visual grounding, termed **MoniRefer**, which contains 411,128 natural language descriptions of 136,018 objects collected from multiple complex traffic intersections in the real world. Each object is annotated with over 10 rich semantic attributes to enhance linguistic diversity and contextual understanding. To construct a high-quality dataset, both instance bounding boxes and linguistic descriptions generated through human annotation and ChatGPT-assisted, are refined and manually verified. MoniRefer fills the gap in 3DVG research under real-world roadside surveillance settings and provides a strong data foundation for future studies on intelligent transportation and smart city cognitive intelligence.

Furthermore, we propose **Moni3DVG**, an end-to-end framework that utilizes appearance, optical and geometric features from visual data and linguistics expression to identify the referred object in roadside-view point clouds. The core idea of our method is to identify the 3D bounding box that best matches the natural language description by select-

ing the candidate point closest to the center of the referred object. Comprehensive experiments on MoniRefer demonstrate the effectiveness and superiority of our approach, establishing a new benchmark for 3D visual grounding in outdoor monitoring scenarios.

In summary, our main contributions are as follow:

- We introduce a novel task of 3D visual grounding task for roadside monitoring scenarios that leverages diverse natural language expressions and multi-modal visual data collected from roadside infrastructure sensors, where the LiDAR and cameras are stationary relative to their surroundings.
- We build the first large-scale multi-modal dataset, termed MoniRefer, for roadside-level 3D visual grounding, featuring 136,018 objects collected from multiple complex traffic intersections, along with 411,128 rich and diverse natural language descriptions, contributing a strong data foundation for advancing future studies in intelligent transportation and smart city cognitive intelligence.
- We propose an end-to-end method, dubbed as Moni3DVG, which efficiently aggregates appearance, optical, and geometric information for multi-modal learning and 3D object localization, achieving high-performance roadside-level 3D visual grounding.
- We provide a sufficient benchmark. Extensive experimental results demonstrate that our proposed end-to-end method achieves state-of-the-art performance on the MoniRefer dataset.

2. Related Work

2D Visual Grounding. The goal of 2D visual grounding(2DVG) is to localize a specific region within an image according to a natural language expression. Over the past decade, numerous datasets [29, 46, 47, 73] and methods [14, 28, 36, 40, 52] have driven significant progress in this area. Existing approaches can be broadly categorized into two paradigms: two-stage and one-stage methods.

Table 1. **Comparison of 3D visual grounding datasets**, where "T.S." indicates time series, "Avg." means average, "Fur." denotes furniture, "Photog." refers to photogrammetry, "LLM" means large language model, "MLLM" represents multi-modal LLM, "H/V" refers to human/vehicle, "VRU/V/O" is interpreted as vulnerable road user/vehicle/obstacle, "Hum.-cent" corresponds to human-centric, "Veh.-cent" indicates vehicle-centric, "Infra.-Level" means infrastructure-level.

Dataset	Sensor	Language Form	Range	Target	Outdoor	T.S.	Objects	Expressions	Avg.Length	Vocab	Views	Scene Nums	Task Level	Label	
ScanRefer [6]	RGB-D	Manual	10m	Fur.	<input checked="" type="checkbox"/>	<input checked="" type="checkbox"/>	11.0k	51.6k	20.27	4,197	-	800	Room-Level	3D BBox	
Nr3D [1]	RGB-D	Manual	10m	Fur.	<input checked="" type="checkbox"/>	<input checked="" type="checkbox"/>	5.9k	41.5k	11.4	6,951	-	641	Room-Level	3D BBox	
Sr3D [1]	RGB-D	Templated	10m	Fur.	<input checked="" type="checkbox"/>	<input checked="" type="checkbox"/>	8.9k	83.5k	-	196	-	1,273	Room-Level	3D BBox	
SUNRefer [35]	RGB-D	Manual	10m	Fur.	<input checked="" type="checkbox"/>	<input checked="" type="checkbox"/>	7.7k	38.5k	16.3	5,279	-	7,699	Room-Level	3D BBox	
CityRefer [44]	UAV Photog.	Manual	-	Variety	<input checked="" type="checkbox"/>	<input checked="" type="checkbox"/>	5.9k	35.2k	-	6,683	-	-	City-Level	3D BBox	
STRefer [34]	LiDAR+RGB	Manual	30m	Human	<input checked="" type="checkbox"/>	<input checked="" type="checkbox"/>	3.6k	5.5k	-	-	1	662	Hum.-Cent	3D BBox	
LifeRefer [34]	LiDAR+RGB	Manual	30m	Human	<input checked="" type="checkbox"/>	<input checked="" type="checkbox"/>	11.8k	25.4k	-	-	1	3,172	Hum.-Cent	3D BBox	
Mono3DRefer [76]	RGB	LLM+Manual	102m	H/V	<input checked="" type="checkbox"/>	<input checked="" type="checkbox"/>	8.2k	41.1k	53.24	5,271	1	2,025	Veh.-Cent	2D/3D BBox	
Talk2Car [15]	RGB	Manual	-	H/V	<input checked="" type="checkbox"/>	<input checked="" type="checkbox"/>	10.5k	11.9k	11.01	-	1	9,217	Veh.-Cent	2D BBox	
Talk2Car-3D [41]	LiDAR+RGB	Manual	-	H/V	<input checked="" type="checkbox"/>	<input checked="" type="checkbox"/>	-	8.4k	-	-	1	5,534	Veh.-Cent	3D BBox	
Talk2Lidar [41]	LiDAR+RGB	MLLM+LLM	-	H/V	<input checked="" type="checkbox"/>	<input checked="" type="checkbox"/>	x	-	59.2k	-	-	6	6,419	Veh.-Cent	3D BBox
NuPrompt [59]	RGB	Manual+LLM	-	H/V	<input checked="" type="checkbox"/>	<input checked="" type="checkbox"/>	-	40.1k	-	-	6	34,149	Veh.-Cent	3D BBox	
Ours	LiDAR+RGB	Manual+LLM	50m	VRU/V/O	<input checked="" type="checkbox"/>	<input checked="" type="checkbox"/>	136.0k	411.1k	126.8	8,478	3	12,085	Infra.-Level	2D/3D BBox	

Two-stage methods [23, 24, 38, 45, 66, 74, 77] first generate a set of region proposals and then select the proposal with the highest region-text matching score as the final prediction. To avoid proposal generation and reduce computational cost, one-stage methods [25, 67, 68, 70, 80] have been developed, which densely fuse image and language features to directly regress the target bounding box. However, directly extending these methods to 3D scenes is not feasible due to the sparse, unordered, and irregular nature of point clouds [48, 49], as well as the lack of accurate 3D geometric information in 2D images, which limit their applicability in real-world scenarios such as autonomous driving and roadside monitoring.

3D Visual Grounding. The objective of 3D visual grounding (3DVG) is to localize a target object in a 3D scene based on a linguistic description. Early works such as ScanRefer [6] and ReferIt3D [1], derived from the ScanNet [13], have greatly promoted the progress of 3DVG in indoor environments. Similar to 2DVG, 3DVG methods are also divided into two-stage and single-stage approaches. Two-stage methods follow a detection-then-matching paradigm. Scanrefer [13] firstly utilize a pretrained 3D object detector [50] to generate a set of object proposals and then match these proposals with given linguistic description to identify target object. Instancerefer [75] reformulates this task as instance matching problem. 3DJCG [5] and UniT3D [9] introduce dense captioning as an auxiliary task. Transformer-based models [22, 26, 78] have also been explored. In contrast, single-stage method 3D-SPS [42] directly deduces target object from point clouds, without relying on the performance of 3D object detector. BUTD-DETR [27] encodes bounding box proposal and decodes objects from contextual features. EDA [62] introduces a text decoupling module to parse linguistic sentence into multiple semantic components. MCLN [51] utilizes a 3D referring expression segmentation task to facilitate collaborative Learning. TSP3D [19] leverages multi-level sparse convolutional

architecture to achieve efficient 3DVG. These approaches and datasets are all based on RGB-D scans in static indoor scenarios, where the perception range of camera is up to 5 meters. Therefore, Cityrefer [44] proposes to perform city-level 3DVG. Wildrefer [34] focuses on human-centric activities. Other datasets [15, 41, 76] focus on 3DVG in outdoor autonomous driving scenes. However, these datasets tend to emphasize vehicles while neglect vulnerable road users (VRUs) related to the situational awareness of autonomous vehicles, such as various cyclists and pedestrians. Besides, sensors mounted on vehicle rooftops are prone to occlusion and limited field-of-view. In this paper, our work focuses on 3D visual grounding for outdoor monitoring scenarios where sensors are stationary relative to their surroundings.

Infrastructure-based 3D Object Detection. 3D object detection is fundamental to autonomous vehicles and intelligent transportation systems. Significant progress has been made in vehicle-centric 3D detection with the development of large-scale datasets [4, 18, 54] and advanced methods [8, 31, 33, 53, 57, 60, 69, 79]. Nevertheless, ego-vehicle sensors suffer from blind spots due to occlusions and limited perception range, which can compromise detection accuracy and driving safety. Roadside perception, offering far-reaching views and reduced blind spots, has therefore attracted increasing attention in intelligent transportation and smart city applications. Recent public datasets [12, 21, 43, 71, 72] have facilitated the emergence of infrastructure-based 3D detection methods [64, 65, 81], such as CBR [17], which enables calibration-free perception via decoupled feature reconstruction, MonoGAE [65], which leverages implicit roadside ground information and high-dimensional semantic features for improved accuracy, and BEVHeight [64], which predicts object height and projects 2D features to 3D space. However, these approaches focus on detecting all candidate objects in a scene and do not support grounding a specific object based on textual descriptions. Motivated by this limitation, in this pa-

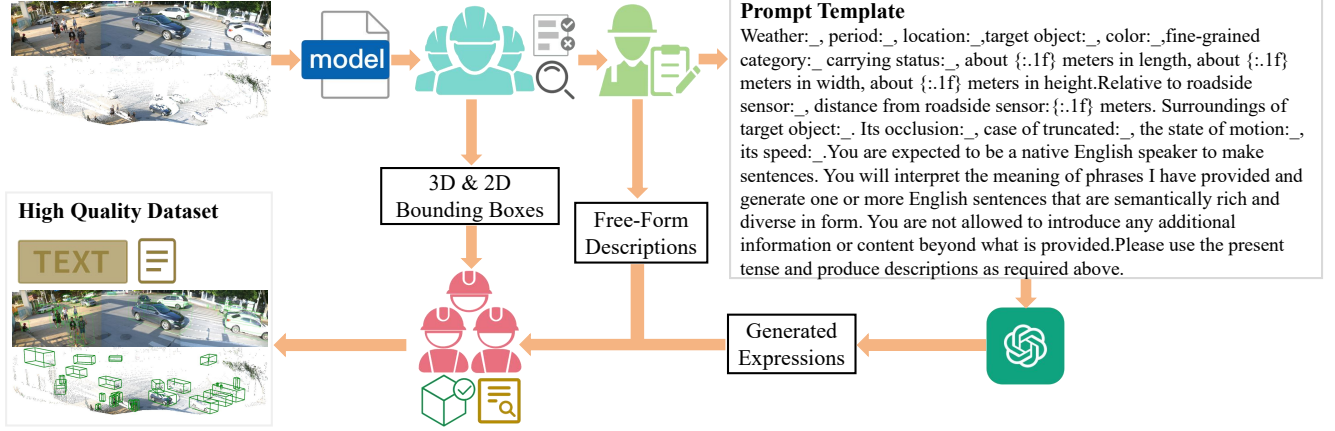


Figure 2. **Our data collection pipeline.** For instance bounding boxes, we employ a pretrained object detector to generate preliminary annotations of objects, followed by manual inspection and refinement. For natural language expressions, annotators are required to provide diverse attributes for each object while labeling the 3D bounding boxes. Then, we obtain semantically rich and diverse textual descriptions by combining manual annotation with LLM-assisted generation.

per, we propose to explore the impact of natural language expressions with multiple attributes on infrastructure-based 3D object detection.

3. MoniRefer Dataset

As shown in Table 1, previous ScanRefer [6], Sr3D [1], Nr3D [1], and SUNRefer [35], concentrate on pre-scanned indoor scenes. Recent efforts such as STRefer [34], LifeRefer [34], Talk2Lidar [41], Talk2Car3D [41], NuPrompt [59], and Mono3DRefer [76] extend 3DVG to outdoor settings, but largely focus on autonomous driving or human-centric activities. To advance the boarder application of 3DVG in outdoor environments, we build a large-scale, multi-modal dataset captured by real-world infrastructure sensors. And we present detailed data acquisition in Sec.3.1, data annotations in Sec.3.2, and dataset statistics in Sec.3.3.



Figure 3. **Sensors Setup and Annotation Area.** (a) showcases the sensor layout of multi-source data acquisition platform. (b) demonstrates the effective annotation range composed of four sensors.

3.1. Data Acquisition

Sensors Setup. To capture large-scale multi-modal data across highly dynamic and complex traffic intersections,

we deploy a multi-source sensing platform, as illustrated in Fig. 3 (a). The system integrates four heterogeneous sensors: one 128-beam mechanical-scanning LiDAR and three identical industrial cameras. Detailed specifications are as follows:

- **LiDAR:** OUSTER OS-1-128, 128 beams, 10Hz, 128×1024 resolution, 360° horizontal FOV, $-22.5^\circ \sim +22.5^\circ$ vertical FOV, and ≤ 170 m range.
- **Industrial cameras:** HIKVISION MV-CA023-10GC with MVL-KF1228M-12MP lens, 10Hz, 1920×1200 resolution, $-29.9^\circ \sim +29.9^\circ$ horizontal FOV, $-23.1^\circ \sim +23.1^\circ$ vertical FOV, equipped with a $1/1.2''$ CMOS sensor.

Synchronization and Calibration. To achieve precise temporal alignment across heterogeneous sensors, we adopt the Precision Time Protocol (PTP) [16], ensuring sub-millisecond synchronization accuracy. High-quality multi-modal data acquisition further requires accurate spatial calibration. Our pipeline involves three coordinate systems: the high-precision point cloud coordinate system, the camera coordinate system, and the LiDAR coordinate system. First, we estimate each camera's intrinsic parameters using OpenCV [3] with a set of chessboard-pattern images. Next, we obtain LiDAR extrinsics by jointly scanning the same scene with a high-precision 3D laser scanner and the LiDAR. We then compute camera extrinsics by detecting corresponding corners in both camera images and the high-precision point cloud using OpenCV. With all intrinsic and extrinsic parameters estimated, transformations among all sensor coordinate systems are fully established, enabling accurate cross-modal fusion.



Figure 4. (a)-(d) present word clouds of terms corresponding to unique words across the dataset, color, coarse-grained object categories, and fine-grained object categories in the MoniRefer dataset, respectively. The fonts size reflects the occurrence frequency of each term in the descriptions.

Data Collection. To enhance the diversity and complexity of our dataset, we deployed our data collection platform at 15 distinct locations across 5 real-world traffic intersections, continuously collecting data over a period of one month. The resulting dataset ultimately comprises 12,085 frames, covering a wide variety of weather conditions (cloudy, overcast, sunny, windy), times of day (morning, afternoon, dusk), intersection types (crossroads, T-junctions, roundabouts), traffic densities (with or without traffic lights, crowded, normal, sparse), and geographic settings (urban, suburban, rural). To enable precise multi-modal fusion, we utilized the accurately calibrated intrinsic and extrinsic parameter matrices to transform the coordinate system and extract color information for each point in every LiDAR frame, yielding a high-fidelity pseudo-color point cloud representation. This extensive and richly annotated dataset not only supports infrastructure-level 2D/3D object detection for vehicles and vulnerable road users, but also surpasses existing 3D visual grounding datasets in both scale and environmental diversity.

3.2. Data Annotations

Annotation Area. Leveraging precise time synchronization and multi-sensor calibration, data from LiDAR and RGB cameras can be jointly annotated, substantially improving labeling accuracy, particularly for distant objects. We define an effective annotation range of 50m, which corresponds to the area simultaneously observable by LiDAR and cameras, as shown in Fig. 3 (b). All objects of interest within this range are systematically annotated to ensure consistent coverage across the dataset.

Annotation Rule. Our dataset includes 12 object categories: car, van, bus, coach, truck, pedestrian, cyclist, tricycle, motorcyclist, electric moped rider, stroller and obstacle. Each object is labeled with a 7-DoF 3D bounding box $(x, y, z, l, w, h, \theta)$, where (x, y, z) denotes the center coordinates, (l, w, h) represents length, width, and height, and θ indicates orientation. Beyond geometric annotations, we provide more than 10 types of attributes information for each object, such as period, location, color, position, orientation, surrounding, motion, speed, and so on.

Annotation Process. To cover the dataset efficiently while reducing inter-frame redundancy, we sample frames from the raw data at intervals of one every ten frames. We adopt a semi-automatic annotation pipeline to get 3D boxes and natural language descriptions, as depicted in Fig. 2: **For 3D bounding boxes**, we first generate proposals using a pretrained object detection model, followed by manual inspection and refinement through multiple quality validation cycles conducted by 17 trained annotators. This ensures that each bounding box accurately represents the corresponding real-world object. **For 2D bounding boxes**, we project the manually verified 3D bounding boxes onto the images of three views using the calibrated high-precision parameter matrices. **For referring expressions**, we employ a hybrid human-and-LLM approach. First, annotators are required to provide more than ten critical attributes for each object in the scene while labeling the 3D bounding boxes. These attributes offer more discriminative cues for ambiguous objects, enabling more accurate localization. Then, annotators generate natural language descriptions based on these key attributes, such that each description uniquely identifies the target object within the 3D scene. To further enhance linguistic diversity and richness, these attributes are fed into a prompt template and passed to a large language model (ChatGPT) for textual expressions generation. All natural language expressions are manually verified by nine team members to ensure accuracy, uniqueness, and consistency. The entire annotation process spans 13 months. Additionally, all potentially sensitive information, such as vehicle license plates and human faces, are blurred using professional labeling tools to ensure privacy compliance. We provide more details about labeling process in the appendix.

3.3. Dataset Statistics

Table 1 presents an overview of our dataset. We collect 12,085 outdoor monitoring scenes using roadside infrastructure sensors equipped with LiDAR and cameras. In total, annotated objects include vehicles, vulnerable road users (VRUs), and generic obstacles within the 50 meters effective range, covering 12 coarse-grained categories and 49 fine-grained categories. Since more detailed descriptions can provide discriminative features that distinguish the target from other objects within the same category, we gen-

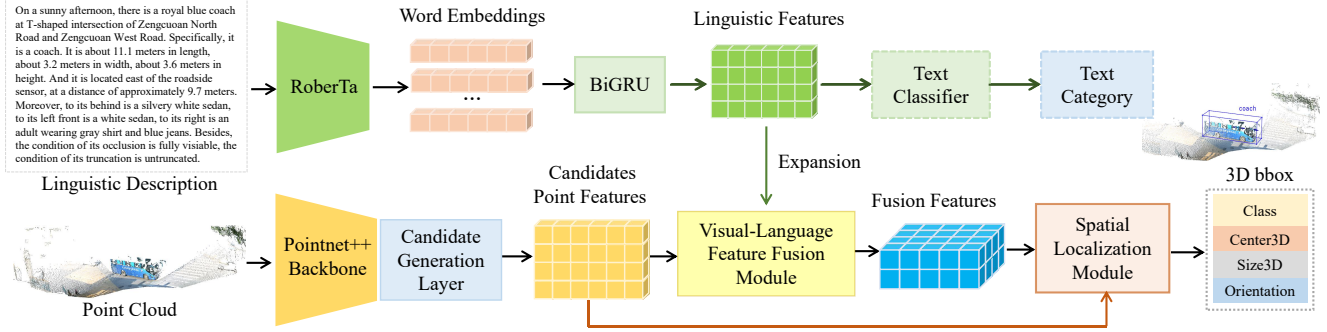


Figure 5. **The overview of Moni3DVG framework.** We formulate the 3DVG task as identifying the candidate point that is closest to the target object center. Specifically, the visual and linguistic encoders extract candidate point representations and textual features from the point clouds and natural language description, respectively. These features are projected into a latent space, where effective cross-modal interaction and fusion are performed to yield enriched multi-modal representations. Finally, the spatial localization module leverages the fused multi-modal features to identify the candidate point nearest to the referred object center and output the 3D bounding box that best matches the referring expression.

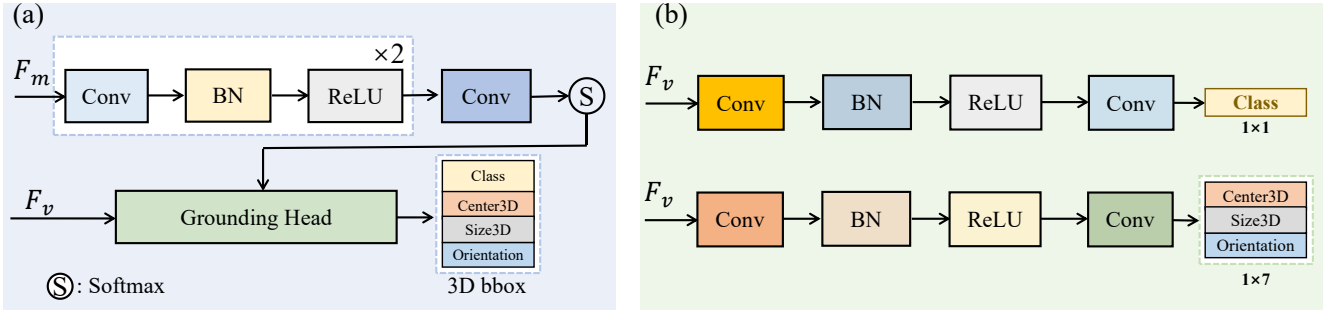


Figure 6. Detail of spatial localization module (a) and grounding head (b). F_m , and F_v denotes multi-modal features and candidate point features, respectively.

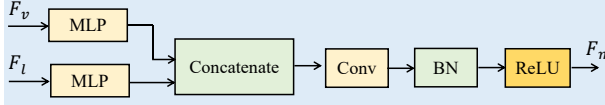


Figure 7. Detail of visual-language feature fusion module. F_v , F_l and F_m represents visual, linguistic and fused multi-modal features, respectively.

erate natural language descriptions based on more than ten attributes for each object through a combination of manual annotation and ChatGPT-assisted generation. Finally, MoniRefer contains 411,128 natural language expressions for 136,018 objects, with an average of 126.78 words per description and a vocabulary of 8,478 unique words. Fig. 4 illustrates different word clouds of our dataset, such as color and object category. Additional detailed statistics and analyses are provided in the supplementary materials.

4. Methodology

In this section, we first formally define a novel grounding task and provide an overview of our proposed framework in Section 4.1. Section 4.2 and Section 4.3 then describe the encoding of visual and textual features from the input point

cloud and the linguistic query, respectively. Section 4.4 presents our multi-modal feature fusion module, which facilitates effective interaction and fusion between visual and linguistic information. Section 4.5 introduces the spatial localization module for identifying the target object corresponding to the input description. Finally, the loss function is detailed in Section 4.6.

4.1. Overview

We introduce the task of 3D visual grounding for outdoor monitoring scenarios (see Fig. 1), where the inputs include a LiDAR point cloud collected from roadside sensors and a diverse linguistic expression referring to a specific object in the scene. Each point encodes geometric information as well as additional appearance and optical attributes. The goal is to predict the 3D bounding box of the object that corresponds to the given description in the physical world.

Inspired by 3DSSD [69], we formulate the task as identifying the candidate point closest to the target object's center among a set of candidate points. To this end, we propose Moni3DVG (see Fig. 5), an end-to-end framework composed of four core components: (1) a visual feature encoder; (2) a linguistic feature encoder; (3) a multi-modal fea-

ture fusion module;(4) a spatial localization module. The visual encoder processes the point cloud to generate representations for candidate points, while the linguistic encoder extracts semantic features from the textual description. These features are then projected into a shared embedding space, where effective cross-modal interaction and fusion are performed to produce enriched multi-modal representations. Finally, the spatial localization module leverages these fused features to predict the target object’s 3D bounding box.

4.2. Visual Feature Encoder

We adopt an enhanced PointNet++ backbone [49] with the fusion sampling strategy and the candidate generation layer from 3DSSD [69] to process the point cloud and extract global features for candidate points. The candidate generation layer outputs a set of center point features denoted as $F_v \in \mathbb{R}^{M \times C_v}$, where M is the maximum number of candidate points and C_v is the feature dimension for each point. These features serve as the visual representation of each candidate point for downstream multi-modal fusion.

4.3. Linguistic Feature Encoder

For the natural language descriptions, we employ a pre-trained RoBERTa-base model [39] to generate word embeddings $F_w \in \mathbb{R}^{L \times C_t}$, where L denotes the number of tokens in the referring expressions and C_t is the vector dimension of each token. The word embeddings are sequentially processed by a bi-directional GRU [11] to capture contextual dependencies within the sentence. The final hidden state of the bi-directional GRU serves as the aggregated linguistic features $F_l \in \mathbb{R}^{1 \times C_l}$ representing the entire textual query, which will be aligned with visual features in the subsequent fusion stage.

4.4. Visual-Language Feature Fusion

To bridge the semantic gap between visual and textual features, visual-language feature fusion module is proposed. As shown in Fig. 7, we first project F_v and F_l into a shared latent space. Then each candidate point feature is concatenated with the corresponding textual feature and processed through a multi-layer perceptron (MLP) to generate fused multi-modal representations $F_m \in \mathbb{R}^{M \times C_m}$, where M indicates the number of candidate points and C_m represents the dimensionality of the fused features. This fusion module enables effective cross-modal interaction, allowing the network to integrate geometric, appearance, optical and linguistic cues for accurate target localization.

4.5. Spatial Localization

The spatial localization module aims to identify the candidate point closest to the center of the ground-truth bounding box corresponding to the textual query. The fused fea-

tures F_m are passed through a single-layer MLP to produce raw scores indicating the likelihood of each candidate point being the target center (Fig. 6 (a)). A softmax function normalizes these scores into localization confidence values $S \in [0, 1]$ for all M points. The point with the highest confidence is selected, and its feature is further processed by grounding head to produce the final 3D bounding box corresponding to the input description (Fig. 6 (b)).

4.6. Loss Function

The overall training process is supervised by five different losses: a reference loss \mathcal{L}_{ref} for referred object localization, a language classification loss \mathcal{L}_{lang} for text to object category classification, and a classification loss \mathcal{L}_{cls} , a regression loss \mathcal{L}_{reg} as well as shifting loss \mathcal{L}_{shift} for 3D bounding box prediction. Specifically, we adopt the classification loss \mathcal{L}_{cls} , regression loss \mathcal{L}_{reg} , and shifting loss \mathcal{L}_{shift} from 3DSSD [69] to supervise candidate points classification, bounding box regression, and center shift prediction, respectively. The language classification loss \mathcal{L}_{lang} is a multi-class cross-entropy loss for predicting the target category based on given description. The reference loss \mathcal{L}_{ref} is formulated as a cross-entropy loss for referred target identification. Finally, the total loss function is computed as a weighted sum of these losses:

$$\mathcal{L} = \lambda_1 \mathcal{L}_{cls} + \lambda_2 \mathcal{L}_{reg} + \lambda_3 \mathcal{L}_{shift} + \lambda_4 \mathcal{L}_{lang} + \lambda_5 \mathcal{L}_{ref}, \quad (1)$$

where λ_i is a balancing factor for weighting the contribution of each loss term.

5. Experiments

5.1. Experimental Setup

Implementation Details. We split our dataset into train/val/test sets with 289,634, 66,981 and 54,513 samples respectively. Our experiments are conducted on six NVIDIA RTX 3090 GPUs using the open-source OpenPCDet [55] codebase. The network is trained for 60 epochs with a batch size of 10, using the Adam optimizer with a learning rate of 1e-4 and weight decay of 1e-4. The learning rate is reduced by a factor of 10 after 35 and 45 epochs. The weights of loss terms, $\lambda_1, \lambda_2, \lambda_3, \lambda_4$, and λ_5 are empirically set to 10, 10, 10, 1, and 1, respectively.

Evaluation Metrics. Following prior 3DVG works [6, 27, 75] in indoor scenes, we adopt Acc@K ($K = 0.25$ or 0.5) as the evaluation metric. Acc@K measures the percentage of predicted bounding boxes whose Intersection over Union (IoU) with the ground-truth exceeds the threshold K .

Baselines. As our work is the first to explore 3D visual grounding in outdoor surveillance scenarios using multi-modal data from infrastructure sensors, there is no related

Table 2. **Comparison results on the MoniRefer validation set.** We measure percentage of predictions whose IoU with the ground truth boxes are greater than 0.25 and 0.5. We report scores of Acc@0.25 and Acc@0.5 for the *Unique* subset, the *Multiple* subset, and *Overall*. The baselines include two-stage and one-stage approaches across different sensor modalities. "Photog." denotes photogrammetry. * means training with ground-truth boxes.

Method	venue	Sensor	Type	Unique		Multiple		Overall	
				Acc@0.25	Acc@0.5	Acc@0.25	Acc@0.5	Acc@0.25	Acc@0.5
CatRandGT	-	LiDAR+RGB	Two-stage	100	100	19.26	19.23	26.66	26.63
3DSSDBest	-	LiDAR+RGB	Two-stage	91.36	68.8	79.48	63.62	80.56	64.09
3DSSDRand	-	LiDAR+RGB	Two-stage	13.93	11.88	5.42	4.92	6.2	5.56
ScanRefer [6]	ECCV2020	RGB-D	Two-stage	7.25	2.43	5.48	3.41	5.64	3.32
Instancerefer* [75]	ICCV2021	RGB-D	Two-stage	53.45	11.06	45.01	7.79	45.78	8.09
Cityrefer* [44]	NeurIPS2023	UAV Photog.	Two-stage	53.54	11.08	44.31	8.99	45.16	9.18
WildRefer [34]	ECCV2024	LiDAR+RGB	One-stage	66.98	16.28	60.47	13.95	61.06	14.16
Moni3DVG(Our)	-	LiDAR+RGB	Two-stage	76.72	57.9	60.43	51.47	61.92	52.06

Table 3. **Performance comparison on the MoniRefer validation set across different distance ranges.** We report Acc@0.25 and Acc@0.5 for *Near* (0–10m), *Medium* (10–30m), and *Far* (30–50m) subsets, as well as *Overall*. "Photog." means photogrammetry. * indicates training with ground-truth boxes.

Method	Sensor	Type	Near (0-10m)		Medium (10-30m)		Far (30-50m)		Overall	
			Acc@0.25	Acc@0.5	Acc@0.25	Acc@0.5	Acc@0.25	Acc@0.5	Acc@0.25	Acc@0.5
CatRandGT	LiDAR+RGB	Two-stage	29.55	29.45	25.77	25.75	27.75	27.75	26.66	26.63
3DSSDBest	LiDAR+RGB	Two-stage	62.54	42.45	83.41	70.74	84.84	56.01	80.56	64.09
3DSSDRand	LiDAR+RGB	Two-stage	4.58	4.06	7.11	6.50	3.9	3.03	6.2	5.56
ScanRefer [6]	RGB-D	Two-stage	14.52	8.66	4.92	2.93	0.73	0.2	5.64	3.32
Instancerefer* [75]	RGB-D	Two-stage	58.62	18.15	50.9	7.74	13.51	0.6	45.78	8.09
Cityrefer* [44]	UAV Photog.	Two-stage	61.72	24.52	49.49	7.97	12.79	0.58	45.16	9.18
WildRefer [34]	LiDAR+RGB	One-stage	64.18	20.41	70.64	12.17	26.83	7.03	61.06	14.16
Moni3DVG(Our)	LiDAR+RGB	Two-stage	52.78	36.87	65.16	57.88	56.73	41.69	61.92	52.06

work for absolutely fair comparison. To explore the difficulty of this task and verify the effectiveness of our approach, we therefore design several baselines and validate these methods under a unified metrics.

CatRandGT. This baseline randomly selects a ground-truth box of the same category as the referred object, serving to estimate the inherent difficulty of the task and dataset. It evaluates grounding performance when only object category information is available, while all other contextual and linguistic cues are disregarded.

3DSSDRand. This baseline randomly chooses a predicted bounding box with the correct semantic class from proposals generated by 3DSSD detector [69]. In contrast to CatRandGT, its performance is highly dependent on the quality of proposals from object detectors.

3DSSDBest. This baseline selects the predicted proposal with the highest IoU with the ground-truth box among all 3DSSD predictions, providing the upper bound on how well the two-stage methods work for our novel task.

Existing 3DVG Methods. In addition to the above baselines, We also evaluate several state-of-the-art 3DVG methods based on RGB-D [6, 75], UAV Photogrammetry [44], and LiDAR [34] data, as shown in Table 2.

To investigate the impact of additional information conveyed by input description beyond object category cues, we

evaluate performance of these baselines on "unique" and "multiple" subsets in Table 2. The "unique" subset includes samples in which there is only one object of the relevant category matches expression, whereas the "multiple" subset contains multiple ambiguous instances with the same category. Furthermore, to examine task difficulty and the effect of sensor perception range, we introduce a distance-based analysis with three levels: Near (0–10m), Medium (10–30m), and Far (30–50m), as reported in Table 3. The "Near", "Medium", and "Far" subsets corresponds to cases where the distance between object center and infrastructure sensor falls within 0–10m, 10–30m, and 30–50m, respectively.

5.2. Quantitative Analysis

As shown in Table 2, we evaluate the performance of our model and several baselines on the val set of MoniRefer. CatRandGT achieves 100% accuracy on the *Unique* subset but drops sharply to 19% on the *Multiple* subset, highlighting the challenge posed by multi-object ambiguity in our task. Although 3DSSDRand performs poorly overall, it achieves higher accuracy in *Unique* than in *Multiple* subset, indicating that category information alone can be sufficient when there is only a single object of its class in the scene. A notable performance gap remains between our end-to-end

Table 4. **Ablation study of Moni3DVG with different input modalities on the validation set of the MoniRefer dataset.** We report the percentage of predictions whose IoU with the ground-truth bounding boxes exceeds 0.25 and 0.5. The *Unique* subset contains samples with no distracting objects, while the *Multiple* subset refers to cases with multiple objects of the same category.

Method	Data	Unique		Multiple		Overall	
		Acc@0.25	Acc@0.5	Acc@0.25	Acc@0.5	Acc@0.25	Acc@0.5
Moni3DVG	xyz	76.46	58.4	58.65	49.97	60.28	50.75
Moni3DVG	xyz+intensity	75.95	54.25	59.12	51.36	60.66	51.62
Moni3DVG	xyz+rgb	77.55	60.35	59.31	50.66	60.98	51.55
Moni3DVG	xyz+rgb+intensity	76.72	57.9	60.43	51.47	61.92	52.06

Table 5. **Ablation study of Moni3DVG with different input modalities on the validation set of the MoniRefer dataset under varying distance ranges.** Based on the distance between the referred object and the sensor, samples are divided into *Near* (0–10m), *Medium* (10–30m), *Far* (30–50m) subsets. Acc@0.25 and Acc@0.5 are reported for each subset as well as *Overall*.

Method	Data	Near (0-10m)		Medium (10-30m)		Far (30-50m)		Overall	
		Acc@0.25	Acc@0.5	Acc@0.25	Acc@0.5	Acc@0.25	Acc@0.5	Acc@0.25	Acc@0.5
Moni3DVG	xyz	53.15	40.2	61.85	55.2	60.2	41.85	60.28	50.75
Moni3DVG	xyz+intensity	50.89	38.3	63.57	56.49	57.41	43.46	60.66	51.62
Moni3DVG	xyz+rgb	51.1	37.53	64	57.31	57.37	40.37	60.98	51.55
Moni3DVG	xyz+rgb+intensity	52.78	36.87	65.16	57.88	56.73	41.69	61.92	52.06

Moni3DVG and 3DSSDBest, suggesting substantial room for improvement the match between language expression and the visual concepts. To further demonstrate the novelty of our task and the effectiveness of our approach, we also evaluate several state-of-the-art 3DVG approaches based on different sensor on MoniRefer. ScanRefer, originally designed for indoor 3DVG, performs poorly due to its limited sensing range and the mismatch in data distribution. CityRefer, derived from InstanceRefer and using ground-truth boxes, exhibits similar performance across all subsets. WildRefer, which targets human-centric indoor and outdoor scenarios, is constrained by its accuracy threshold. In contrast, Moni3DVG, specifically designed for outdoor monitoring scenarios, demonstrates strong adaptability and effectiveness under complex and high dynamic traffic environments.

As reported in Table 3, CatRandGT performs slightly better on the *Near* subset than on the *Medium* and *Far* subsets, while 3DSSDRand performs best on the *Medium* subset, indicating that model is biased toward medium-range objects. Both ScanRefer and InstanceRefer, which rely on RGB-D data collected in indoor environments, show decreasing performance as distance increases and perform best on the *Near*(0–10 m) subset. Although CityRefer employs ground-truth bounding boxes, it struggles to handle roadside monitoring scenarios due to inconsistent data distributions. WildRefer, which leverages data from RGB cameras and LiDAR with a maximum sensing range of 30 m, presents a sharp performance drop in the *Far* (30–50 m) subset, and its localization accuracy is further limited by the evaluation threshold. In contrast, our method outperforms all baselines beyond 3DSSDBest, demonstrating

superior performance. Notably, it not only models contextual relations among objects to disambiguate same category instances but also effectively associates semantic information between textual descriptions and scene context, resulting in more accurate target localization. Additional results and analyses on the test set are provided in the supplementary material.

5.3. Qualitative Analysis

Fig. 8 presents visualization results of CatRandGT, 3DSSDRand, 3DSSDBest, ScanRefer, WildRefer, and our Moni3DVG on samples randomly selected from two different scenarios. In these scenes containing multiple objects of the same category, CatRandGT and 3DSSDRand are unable to identify the referred object when relying solely on object category information. ScanRefer fails to predict targets beyond the RGB-D camera’s sensing range (5 m), as the objects lie within the *Medium*(10–30 m) subset. Although WildRefer leverages both LiDAR and RGB inputs, it is designed for human-centric activity scenarios and struggles to accurately localize objects beyond the human category. In contrast, both 3DSSDBest and our method produce correct predictions, where 3DSSDBest serves as the upper bound of our two-stage framework. Notably, our method not only demonstrates a strong capability in handling spatial relations to disambiguate same category objects, but also effectively models semantic correlations between scene context and textual descriptions through multi-modal fusion and interaction, resulting in more accurate target localization. More detailed qualitative analyses are provided in the appendix.

5.4. Ablation Studies

We conduct an ablation study to analyze the contribution of different point cloud features to our model performance. Table 4 reports Acc@0.25 and Acc@0.5 on the *Unique*, *Multiple*, and *Overall*, while Table 5 presents the results on the *Near*, *Medium*, *Far*, and *Overall*. As shown in Table 4, the first row corresponds to using only geometric features(xyz), and introducing optical features (intensity) in the second row leads to consistent performance improvements on the *Overall*. Incorporating appearance features(rgb) in the third row further enhances the results. When all feature modalities(xyz+rgb+intensity) are combined, the model achieves the best performance, demonstrating the complementary nature of geometric, optical, and appearance features. A similar trend is observed in Table 5, where adding either appearance (rgb) or optical (intensity) information improves localization accuracy over the geometry-only baseline, and the best results can be improved by approximately 1%-2% when all features(xyz+rgb+intensity) are used. Results in both tables all demonstrate that integrating multiple feature information consistently enhances the overall target localization performance of the model. More additional ablation analyses are provided in the supplementary material.

6. Conclusion

In this paper, we explore a novel 3D visual grounding for outdoor monitoring scenarios, which aims to localize target objects in 3D space based on natural language expressions and multi-modal visual data captured by roadside infrastructure sensors. We further contribute a high quality large-scale multi-modal dataset for roadside-level 3D visual grounding, which contains 411,128 descriptions for 136,018 objects. Moreover, we propose Moni3DVG, an end-to-end framework that integrates geometric, appearance, and optical information from point clouds and images, enabling effective multi-modal feature learning and accurate 3D object localization. Extensive experiments demonstrate the effectiveness and state-of-the-art performance of our approach. Finally, we hope our dataset and method will advance 3D vision-language research and foster the development of intelligent infrastructure systems and embodied agents capable of human-like recognition.

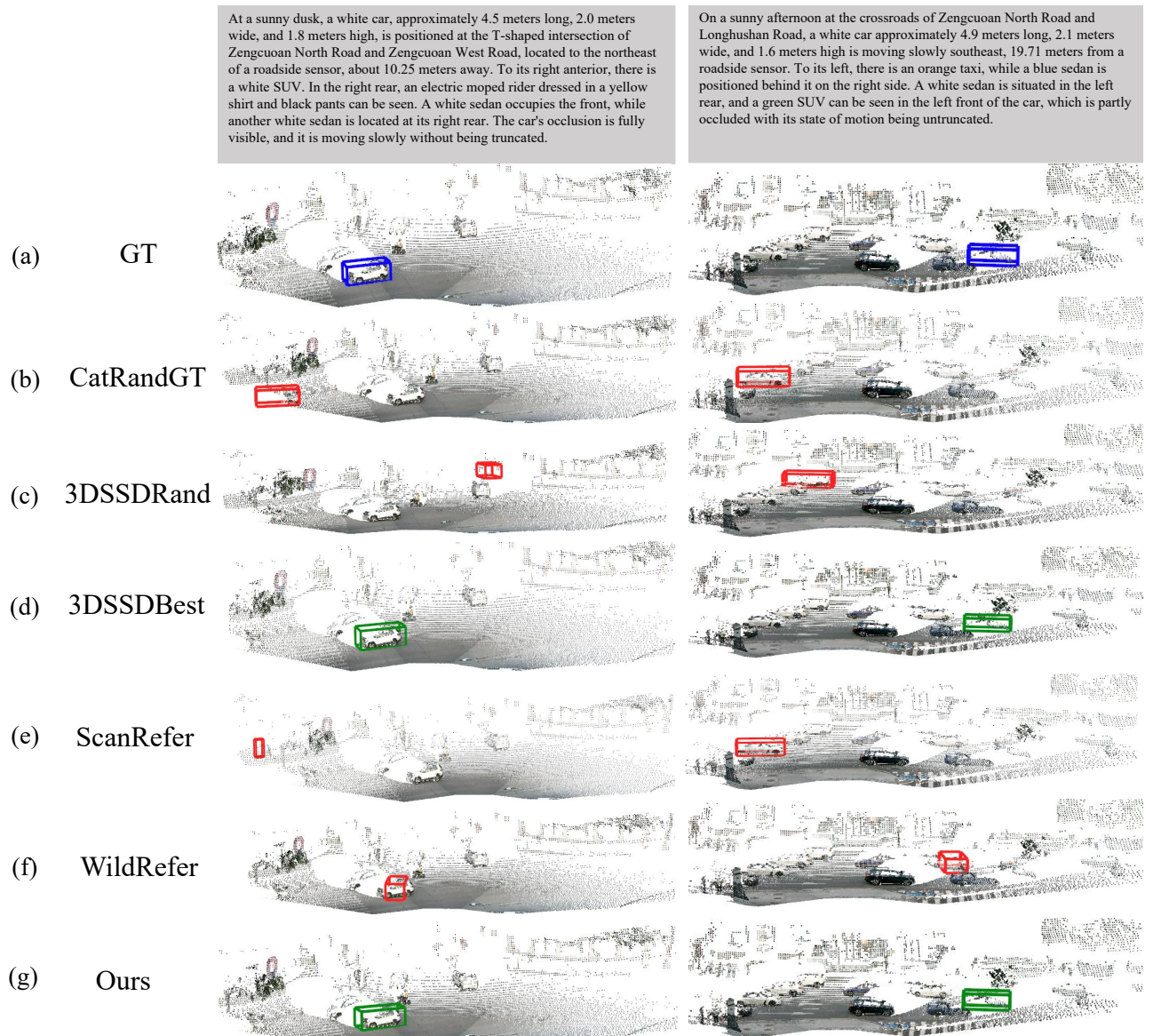


Figure 8. **Qualitative results from baseline methods and our Moni3DVG on MoniRefer dataset.** Blue, green and red boxes denote the ground-truth, right prediction, and wrong prediction, respectively.

References

[1] Panos Achlioptas, Ahmed Abdelreheem, Fei Xia, Mohamed Elhoseiny, and Leonidas Guibas. Referit3d: Neural listeners for fine-grained 3d object identification in real-world scenes. In *ECCV*, pages 422–440. Springer, 2020. [1](#), [3](#), [4](#)

[2] Peter Anderson, Qi Wu, Damien Teney, Jake Bruce, Mark Johnson, Niko Sünderhauf, Ian Reid, Stephen Gould, and Anton Van Den Hengel. Vision-and-language navigation: Interpreting visually-grounded navigation instructions in real environments. In *CVPR*, pages 3674–3683, 2018. [1](#)

[3] Gary Bradski. The opencv library. *Dr. Dobb's Journal: Software Tools for the Professional Programmer*, 25(11):120–123, 2000. [4](#)

[4] Holger Caesar, Varun Bankiti, Alex H Lang, Sourabh Vora, Venice Erin Liong, Qiang Xu, Anush Krishnan, Yu Pan, Giancarlo Baldan, and Oscar Beijbom. nuscenes: A multimodal dataset for autonomous driving. In *CVPR*, pages 11621–11631, 2020. [1](#), [3](#)

[5] Daigang Cai, Lichen Zhao, Jing Zhang, Lu Sheng, and Dong Xu. 3djcg: A unified framework for joint dense captioning and visual grounding on 3d point clouds. In *CVPR*, pages 16464–16473, 2022. [3](#)

[6] Dave Zhenyu Chen, Angel X Chang, and Matthias Nießner. Scanrefer: 3d object localization in rgb-d scans using natural language. In *ECCV*, pages 202–221. Springer, 2020. [1](#), [3](#), [4](#), [7](#), [8](#)

[7] Shizhe Chen, Pierre-Louis Guhur, Makarand Tapaswi, Cordelia Schmid, and Ivan Laptev. Think global, act local: Dual-scale graph transformer for vision-and-language navigation. In *CVPR*, pages 16537–16547, 2022. [1](#)

[8] Yukang Chen, Jianhui Liu, Xiangyu Zhang, Xiaojuan Qi, and Jiaya Jia. Voxelnext: Fully sparse voxelnet for 3d object detection and tracking. In *CVPR*, pages 21674–21683, 2023. [1](#), [3](#)

[9] Zhenyu Chen, Ronghang Hu, Xinlei Chen, Matthias Nießner, and Angel X Chang. Unit3d: A unified transformer for 3d dense captioning and visual grounding. In *ICCV*, pages 18109–18119, 2023. [3](#)

[10] Wenhao Cheng, Junbo Yin, Wei Li, Ruigang Yang, and Jianbing Shen. Language-guided 3d object detection in point cloud for autonomous driving. *arXiv preprint arXiv:2305.15765*, 2023. [1](#)

[11] Junyoung Chung, Caglar Gulcehre, KyungHyun Cho, and Yoshua Bengio. Empirical evaluation of gated recurrent neural networks on sequence modeling. *arXiv preprint arXiv:1412.3555*, 2014. [7](#)

[12] Christian Creß, Walter Zimmer, Leah Strand, Maximilian Fortkord, Siyi Dai, Venkatnarayanan Lakshminarasimhan, and Alois Knoll. A9-dataset: Multi-sensor infrastructure-based dataset for mobility research. In *IEEE Intelligent Vehicles Symposium*, pages 965–970. IEEE, 2022. [3](#)

[13] Angela Dai, Angel X Chang, Manolis Savva, Maciej Halber, Thomas Funkhouser, and Matthias Nießner. Scannet: Richly-annotated 3d reconstructions of indoor scenes. In *CVPR*, pages 5828–5839, 2017. [3](#)

[14] Chaorui Deng, Qi Wu, Qingyao Wu, Fuyuan Hu, Fan Lyu, and Mingkui Tan. Visual grounding via accumulated attention. In *CVPR*, pages 7746–7755, 2018. [1](#), [2](#)

[15] Thierry Deruyttere, Simon Vandenhende, Dusan Gruijicic, Luc Van Gool, and Marie-Francine Moens. Talk2car: Taking control of your self-driving car. *arXiv preprint arXiv:1909.10838*, 2019. [1](#), [3](#)

[16] John C Eidson, Mike Fischer, and Joe White. Ieee-1588™ standard for a precision clock synchronization protocol for networked measurement and control systems. In *Proceedings of the 34th annual precise time and time interval systems and applications meeting*, pages 243–254, 2002. [4](#)

[17] Siqi Fan, Zhe Wang, Xiaoliang Huo, Yan Wang, and Jingjing Liu. Calibration-free bev representation for infrastructure perception. In *IROS*, pages 9008–9013. IEEE, 2023. [3](#)

[18] Andreas Geiger, Philip Lenz, and Raquel Urtasun. Are we ready for autonomous driving? the kitti vision benchmark suite. In *CVPR*, pages 3354–3361. IEEE, 2012. [1](#), [3](#)

[19] Wenxuan Guo, Xiuwei Xu, Ziwei Wang, Jianjiang Feng, Jie Zhou, and Jiwen Lu. Text-guided sparse voxel pruning for efficient 3d visual grounding. In *CVPR*, pages 3666–3675, 2025. [1](#), [3](#)

[20] Yanjiang Guo, Jianke Zhang, Xiaoyu Chen, Xiang Ji, Yen-Jen Wang, Yucheng Hu, and Jianyu Chen. Improving vision-language-action model with online reinforcement learning. *arXiv preprint arXiv:2501.16664*, 2025. [1](#)

[21] Ruiyang Hao, Siqi Fan, Yingru Dai, Zhenlin Zhang, Chenxi Li, Yuntian Wang, Haibao Yu, Wenxian Yang, Jirui Yuan, and Zaiqing Nie. Rcooper: A real-world large-scale dataset for roadside cooperative perception. In *CVPR*, pages 22347–22357, 2024. [1](#), [3](#)

[22] Dailan He, Yusheng Zhao, Junyu Luo, Tianrui Hui, Shaofei Huang, Aixi Zhang, and Si Liu. Transrefer3d: Entity-and-relation aware transformer for fine-grained 3d visual grounding. In *ACM MM*, pages 2344–2352, 2021. [3](#)

[23] Richang Hong, Daqing Liu, Xiaoyu Mo, Xiangnan He, and Hanwang Zhang. Learning to compose and reason with language tree structures for visual grounding. *IEEE TPAMI*, 44(2):684–696, 2019. [3](#)

[24] Ronghang Hu, Marcus Rohrbach, Jacob Andreas, Trevor Darrell, and Kate Saenko. Modeling relationships in referential expressions with compositional modular networks. In *CVPR*, pages 1115–1124, 2017. [3](#)

[25] Binbin Huang, Dongze Lian, Weixin Luo, and Shenghua Gao. Look before you leap: Learning landmark features for one-stage visual grounding. In *CVPR*, pages 16888–16897, 2021. [3](#)

[26] Shijia Huang, Yilun Chen, Jiaya Jia, and Liwei Wang. Multi-view transformer for 3d visual grounding. In *CVPR*, pages 15524–15533, 2022. [3](#)

[27] Ayush Jain, Nikolaos Gkanatsios, Ishita Mediratta, and Katefrina Fragkiadaki. Bottom up top down detection transformers for language grounding in images and point clouds. In *ECCV*, pages 417–433. Springer, 2022. [1](#), [3](#), [7](#)

[28] Aishwarya Kamath, Mannat Singh, Yann LeCun, Gabriel Synnaeve, Ishan Misra, and Nicolas Carion. Mdetr-modulated detection for end-to-end multi-modal understanding. In *ICCV*, pages 1780–1790, 2021. [1](#), [2](#)

[29] Sahar Kazemzadeh, Vicente Ordonez, Mark Matten, and Tamara Berg. Referitgame: Referring to objects in photographs of natural scenes. In *EMNLP*, pages 787–798, 2014. 2

[30] Moo Jin Kim, Karl Pertsch, Siddharth Karamchetti, Ted Xiao, Ashwin Balakrishna, Suraj Nair, Rafael Rafailov, Ethan Foster, Grace Lam, Pannag Sanketi, et al. Openvla: An open-source vision-language-action model. *arXiv preprint arXiv:2406.09246*, 2024. 1

[31] Alex H Lang, Sourabh Vora, Holger Caesar, Lubing Zhou, Jiong Yang, and Oscar Beijbom. Pointpillars: Fast encoders for object detection from point clouds. In *CVPR*, pages 12697–12705, 2019. 1, 3

[32] Fuhao Li, Huan Jin, Bin Gao, Liaoyuan Fan, Lihui Jiang, and Long Zeng. Nugrounding: A multi-view 3d visual grounding framework in autonomous driving. *arXiv preprint arXiv:2503.22436*, 2025. 1

[33] Tingting Liang, Hongwei Xie, Kaicheng Yu, Zhongyu Xia, Zhiwei Lin, Yongtao Wang, Tao Tang, Bing Wang, and Zhi Tang. Bevfusion: A simple and robust lidar-camera fusion framework. *NeurIPS*, 35:10421–10434, 2022. 3

[34] Zhenxiang Lin, Xidong Peng, Peishan Cong, Ge Zheng, Yujin Sun, Yuenan Hou, Xinge Zhu, Sibei Yang, and Yuexin Ma. Wildrefer: 3d object localization in large-scale dynamic scenes with multi-modal visual data and natural language. In *ECCV*, pages 456–473. Springer, 2024. 1, 3, 4, 8

[35] Haolin Liu, Anran Lin, Xiaoguang Han, Lei Yang, Yizhou Yu, and Shuguang Cui. Refer-it-in-rgbd: A bottom-up approach for 3d visual grounding in rgbd images. In *CVPR*, pages 6032–6041, 2021. 3, 4

[36] Shilong Liu, Shijia Huang, Feng Li, Hao Zhang, Yaoyuan Liang, Hang Su, Jun Zhu, and Lei Zhang. Dq-detr: Dual query detection transformer for phrase extraction and grounding. In *AAAI*, pages 1728–1736, 2023. 2

[37] Shubo Liu, Hongsheng Zhang, Yuankai Qi, Peng Wang, Yan-ning Zhang, and Qi Wu. Aerialvln: Vision-and-language navigation for uavs. In *ICCV*, pages 15384–15394, 2023. 1

[38] Xihui Liu, Zihao Wang, Jing Shao, Xiaogang Wang, and Hongsheng Li. Improving referring expression grounding with cross-modal attention-guided erasing. In *CVPR*, pages 1950–1959, 2019. 1, 3

[39] Yinhan Liu, Myle Ott, Naman Goyal, Jingfei Du, Mandar Joshi, Danqi Chen, Omer Levy, Mike Lewis, Luke Zettlemoyer, and Veselin Stoyanov. Roberta: A robustly optimized bert pretraining approach. *arXiv preprint arXiv:1907.11692*, 2019. 7

[40] Yongfei Liu, Bo Wan, Xiaodan Zhu, and Xuming He. Learning cross-modal context graph for visual grounding. In *AAAI*, pages 11645–11652, 2020. 2

[41] Yuhang Liu, Boyi Sun, Yishuo Wang, Jing Yang, Xingxia Wang, and Fei-Yue Wang. Talk to parallel lidars: A human-lidar interaction method based on 3d visual grounding. In *ECCV*, pages 305–321. Springer, 2024. 3, 4

[42] Junyu Luo, Jiahui Fu, Xianghao Kong, Chen Gao, Haibing Ren, Hao Shen, Huaxia Xia, and Si Liu. 3d-sps: Single-stage 3d visual grounding via referred point progressive selection. In *CVPR*, pages 16454–16463, 2022. 1, 3

[43] Jonas Mirlach, Lei Wan, Andreas Wiedholz, Hannan Ejaz Keen, and Andreas Eich. R-livit: A lidar-visual-thermal dataset enabling vulnerable road user focused roadside perception. *arXiv preprint arXiv:2503.17122*, 2025. 3

[44] Taiki Miyanishi, Fumiya Kitamori, Shuhei Kurita, Jungdae Lee, Motoaki Kawanabe, and Nakamasa Inoue. Cityrefer: Geography-aware 3d visual grounding dataset on city-scale point cloud data. *NeurIPS*, 36:77758–77770, 2023. 3, 8

[45] Varun K Nagaraja, Vlad I Morariu, and Larry S Davis. Modeling context between objects for referring expression understanding. In *ECCV*, pages 792–807. Springer, 2016. 3

[46] Varun K Nagaraja, Vlad I Morariu, and Larry S Davis. Modeling context between objects for referring expression understanding. In *ECCV*, pages 792–807. Springer, 2016. 1, 2

[47] Bryan A Plummer, Liwei Wang, Chris M Cervantes, Juan C Caicedo, Julia Hockenmaier, and Svetlana Lazebnik. Flickr30k entities: Collecting region-to-phrase correspondences for richer image-to-sentence models. In *ICCV*, pages 2641–2649, 2015. 1, 2

[48] Charles R Qi, Hao Su, Kaichun Mo, and Leonidas J Guibas. Pointnet: Deep learning on point sets for 3d classification and segmentation. In *CVPR*, pages 652–660, 2017. 3

[49] Charles Ruizhongtai Qi, Li Yi, Hao Su, and Leonidas J Guibas. Pointnet++: Deep hierarchical feature learning on point sets in a metric space. *NeurIPS*, 30, 2017. 3, 7

[50] Charles R Qi, Or Litany, Kaiming He, and Leonidas J Guibas. Deep hough voting for 3d object detection in point clouds. In *ICCV*, pages 9277–9286, 2019. 3

[51] Zhipeng Qian, Yiwei Ma, Zhekai Lin, Jiayi Ji, Xiaowu Zheng, Xiaoshuai Sun, and Rongrong Ji. Multi-branch collaborative learning network for 3d visual grounding. In *ECCV*, pages 381–398. Springer, 2024. 3

[52] Fengyuan Shi, Ruopeng Gao, Weilin Huang, and Limin Wang. Dynamic mdetr: A dynamic multimodal transformer decoder for visual grounding. *IEEE TPAMI*, 46(2):1181–1198, 2023. 1, 2

[53] Shaoshuai Shi, Xiaogang Wang, and Hongsheng Li. Pointrcnn: 3d object proposal generation and detection from point cloud. In *CVPR*, pages 770–779, 2019. 1, 3

[54] Pei Sun, Henrik Kretzschmar, Xerxes Dotiwalla, Aurelien Chouard, Vijaysai Patnaik, Paul Tsui, James Guo, Yin Zhou, Yuning Chai, Benjamin Caine, et al. Scalability in perception for autonomous driving: Waymo open dataset. In *CVPR*, pages 2446–2454, 2020. 3

[55] OD Team et al. Openpcdet: An open-source toolbox for 3d object detection from point clouds, 2020. 7

[56] Quan Vuong, Sergey Levine, Homer Rich Walke, Karl Pertsch, Anikait Singh, Ria Doshi, Charles Xu, Jianlan Luo, Liam Tan, Dhruv Shah, et al. Open x-embodiment: Robotic learning datasets and rt-x models. In *CoRL*, 2023. 1

[57] Yue Wang, Vitor Campagnolo Guizilini, Tianyuan Zhang, Yilun Wang, Hang Zhao, and Justin Solomon. Detr3d: 3d object detection from multi-view images via 3d-to-2d queries. In *CoRL*, pages 180–191. PMLR, 2022. 3

[58] Zhiqiang Wang, Hao Zheng, Yunshuang Nie, Wenjun Xu, Qingwei Wang, Hua Ye, Zhe Li, Kaidong Zhang, Xuewen Cheng, Wanxi Dong, et al. All robots in one: A new standard

and unified dataset for versatile, general-purpose embodied agents. *arXiv preprint arXiv:2408.10899*, 2024. 1

[59] Dongming Wu, Wencheng Han, Yingfei Liu, Tiancai Wang, Cheng-zhong Xu, Xiangyu Zhang, and Jianbing Shen. Language prompt for autonomous driving. In *AAAI*, pages 8359–8367, 2025. 3, 4

[60] Hai Wu, Chenglu Wen, Shaoshuai Shi, Xin Li, and Cheng Wang. Virtual sparse convolution for multimodal 3d object detection. In *CVPR*, pages 21653–21662, 2023. 1, 3

[61] Kun Wu, Chengkai Hou, Jiaming Liu, Zhengping Che, Xiaozhu Ju, Zhuqin Yang, Meng Li, Yinuo Zhao, Zhiyuan Xu, Guang Yang, et al. Robomind: Benchmark on multi-embodiment intelligence normative data for robot manipulation. *arXiv preprint arXiv:2412.13877*, 2024. 1

[62] Yanmin Wu, Xinhua Cheng, Renrui Zhang, Zesen Cheng, and Jian Zhang. Eda: Explicit text-decoupling and dense alignment for 3d visual grounding. In *CVPR*, pages 19231–19242, 2023. 1, 3

[63] Zhenyu Wu, Yuheng Zhou, Xiuwei Xu, Ziwei Wang, and Haibin Yan. Momanipvla: Transferring vision-language-action models for general mobile manipulation. In *CVPR*, pages 1714–1723, 2025. 1

[64] Lei Yang, Kaicheng Yu, Tao Tang, Jun Li, Kun Yuan, Li Wang, Xinyu Zhang, and Peng Chen. Bevheight: A robust framework for vision-based roadside 3d object detection. In *CVPR*, pages 21611–21620, 2023. 3

[65] Lei Yang, Xinyu Zhang, Jiaxin Yu, Jun Li, Tong Zhao, Li Wang, Yi Huang, Chuang Zhang, Hong Wang, and Yiming Li. Monogae: Roadside monocular 3d object detection with ground-aware embeddings. *TITS*, 25(11):17587–17601, 2024. 3

[66] Sibei Yang, Guanbin Li, and Yizhou Yu. Dynamic graph attention for referring expression comprehension. In *ICCV*, pages 4644–4653, 2019. 1, 3

[67] Zhengyuan Yang, Boqing Gong, Liwei Wang, Wenbing Huang, Dong Yu, and Jiebo Luo. A fast and accurate one-stage approach to visual grounding. In *ICCV*, pages 4683–4693, 2019. 1, 3

[68] Zhengyuan Yang, Tianlang Chen, Liwei Wang, and Jiebo Luo. Improving one-stage visual grounding by recursive sub-query construction. In *Computer Vision–ECCV 2020: 16th European Conference, Glasgow, UK, August 23–28, 2020, Proceedings, Part XIV 16*, pages 387–404. Springer, 2020. 3

[69] Zetong Yang, Yanan Sun, Shu Liu, and Jiaya Jia. 3dssd: Point-based 3d single stage object detector. In *CVPR*, pages 11040–11048, 2020. 3, 6, 7, 8

[70] Ruilin Yao, Shengwu Xiong, Yichen Zhao, and Yi Rong. Visual grounding with multi-modal conditional adaptation. In *ACM MM*, pages 3877–3886, 2024. 3

[71] Xiaoqing Ye, Mao Shu, Hanyu Li, Yifeng Shi, Yingying Li, Guangjie Wang, Xiao Tan, and Errui Ding. Rope3d: The roadside perception dataset for autonomous driving and monocular 3d object detection task. In *CVPR*, pages 21341–21350, 2022. 1, 3

[72] Haibao Yu, Yizhen Luo, Mao Shu, Yiyi Huo, Zebang Yang, Yifeng Shi, Zhenglong Guo, Hanyu Li, Xing Hu, Jirui Yuan, et al. Dair-v2x: A large-scale dataset for vehicle-infrastructure cooperative 3d object detection. In *CVPR*, pages 21361–21370, 2022. 1, 3

[73] Licheng Yu, Patrick Poirson, Shan Yang, Alexander C Berg, and Tamara L Berg. Modeling context in referring expressions. In *ECCV*, pages 69–85. Springer, 2016. 1, 2

[74] Licheng Yu, Zhe Lin, Xiaohui Shen, Jimei Yang, Xin Lu, Mohit Bansal, and Tamara L Berg. Mattnet: Modular attention network for referring expression comprehension. In *CVPR*, pages 1307–1315, 2018. 1, 3

[75] Zhihao Yuan, Xu Yan, Yinghong Liao, Ruimao Zhang, Sheng Wang, Zhen Li, and Shuguang Cui. Instancerefer: Cooperative holistic understanding for visual grounding on point clouds through instance multi-level contextual referring. In *ICCV*, pages 1791–1800, 2021. 1, 3, 7, 8

[76] Yang Zhan, Yuan Yuan, and Zhitong Xiong. Mono3dvg: 3d visual grounding in monocular images. In *AAAI*, pages 6988–6996, 2024. 1, 3, 4

[77] Hanwang Zhang, Yulei Niu, and Shih-Fu Chang. Grounding referring expressions in images by variational context. In *CVPR*, pages 4158–4166, 2018. 3

[78] Lichen Zhao, Daigang Cai, Lu Sheng, and Dong Xu. 3dvg-transformer: Relation modeling for visual grounding on point clouds. In *ICCV*, pages 2928–2937, 2021. 1, 3

[79] Yin Zhou and Oncel Tuzel. Voxelnet: End-to-end learning for point cloud based 3d object detection. In *CVPR*, pages 4490–4499, 2018. 3

[80] Yiyi Zhou, Rongrong Ji, Gen Luo, Xiaoshuai Sun, Jinsong Su, Xinghao Ding, Chia-Wen Lin, and Qi Tian. A real-time global inference network for one-stage referring expression comprehension. *TNNLS*, 34(1):134–143, 2021. 3

[81] Walter Zimmer, Joseph Birkner, Marcel Brucker, Huu Tung Nguyen, Stefan Petrovski, Bohan Wang, and Alois C Knoll. Infradet3d: Multi-modal 3d object detection based on roadside infrastructure camera and lidar sensors. In *IEEE Intelligent Vehicles Symposium*, pages 1–8. IEEE, 2023. 1, 3